Growth behavior, electronic structure, and vibrational properties of Si_nY anion clusters ($n = 4$–20): Metal atom as linker and endohedral dopant

S. Jaiswal,[1,2] Vasudeo P. Babar,[1] and Vijay Kumar[1,3]

[1]*Dr. Vijay Kumar Foundation, 1969 Sector 4, Gurgaon 122001, Haryana, India*

[2]*Department of Physics, Sunrise University, Alwar, Rajasthan, India*

[3]*Center for Informatics, School of Natural Sciences, Shiv Nadar University, Chithera, Gautum Budh Nagar 203 207, Uttar Pradesh, India*

(Received 14 May 2013; revised manuscript received 18 July 2013; published 12 August 2013)

We report results of *ab initio* calculations on Y-doped anion Si_n clusters with $n = 4$–20. Our results suggest two growth behaviors in the intermediate range of $n = 8$ and 20: (1) There is the formation of *linked* clusters in which a metal atom links two subclusters and (2) where silicon atoms form a cage structure and the metal atom is inside the cage to produce *endohedral* cages of silicon clusters. The cluster structures have been identified by comparing the calculated spectra of the electronic states with the photoemission spectra on anion clusters. Our results suggest that in some cases a higher energy isomer may be present in experiments. We report the calculations of the infrared and Raman spectra as well as the dipole moments, electron affinity, and polarizability that could provide other ways of identifying the growth behavior in these clusters.

DOI: 10.1103/PhysRevB.88.085412 PACS number(s): 36.40.Cg, 36.40.Wa, 73.22.−f

I. INTRODUCTION

Silicon is the most important material for the semiconductor industry, and with continuous miniaturization of the semiconductor devices, there has been great interest in understanding the properties of its nanostructures. Moreover, bulk silicon is not a good emitter of light, but in the early 1990s intense light was observed[1] from porous silicon that created great interest in understanding the optical properties of silicon nanostructures.[2] Over the past two decades, silicon clusters, nanoparticles, and nanowires have been studied extensively, and possibilities have been explored[2] for applications in nanoelectronics, optoelectronics, silicon laser, drug delivery, and sensors. Early work on pure silicon clusters showed prolate structures in the size range of 15–25 atoms[2–4] and thereafter three-dimensional fullerenelike structures in which a few silicon atoms were encapsulated in a fullerenelike cage of silicon. However, in 2001, it was shown that doping of a metal atom changes the atomic structure of silicon clusters completely, and prominent new magic clusters $Zr@Si_{16}$ and $Ti@Si_{16}$ with fullerene and Frank-Kasper (FK) polyhedral structures, respectively, were predicted among others,[5] and these have been subsequently realized in laboratory.[6] These findings created renewed interest in clusters of silicon and other group 14 elements in the hope of finding new species of silicon that could possibly be produced in high abundance. In the past decade, much research has been done to develop and understand the properties of metal-doped silicon nanoclusters and their possible assemblies.

Metal doping makes it possible to prepare size-specific silicon clusters with high abundance and tune the properties that could make them usable for specific applications.[7,8] The structural, electronic, magnetic, and vibrational properties of metal-doped silicon clusters depend on the dopant atom. The metal atom alters the properties of silicon clusters such as the energy gap that, in turn, affects the optical properties. After the first predictions of silicon fullerenes and other polyhedral forms,[5] many theoretical and experimental studies on metal-doped silicon and other group 14 element clusters have been done over the past few years. The detailed photoelectron spectroscopy (PES) studies of Koyasu *et al.*[9] on silicon clusters doped with different metal atoms provide an opportunity to revisit and understand the growth behavior of metal-doped silicon clusters from first-principles calculations. Here, we report results of such a study on Si_nY anion clusters with $n = 4$–20.

Earlier Yang *et al.*[10] investigated geometries, stabilities, and electronic properties of neutral Y-doped Si_n (n = 1–16) clusters using density functional theory. They found that up to $n = 14$, the Y atom occupies a surface site and at $n = 15$, the metal atom drops inside a silicon cage. Kumar *et al.*[11] have studied the stability of the $Y@Si_{20}$ anion cluster and suggested its structure to be a Si_{20} fullerene with 12 pentagonal faces and a Y atom inside the cage. Extensive studies have been done on metal-doped silicon clusters by Kawamura *et al.*[12] who studied the growth behavior of isoelectronic Si_nM ($n =$ 8–16 and $M =$ Ti, Zr, and Hf) clusters. The main growth behavior was predicted to be the one in which the metal atom was exposed lying on a surface site for n up to 12, while for $n = 13$, the metal atom falls inside a cage and is not able to interact, e.g., with a water molecule.[13] The encapsulation of the metal atom in a silicon cage has been found to lead to enhanced stability of these clusters compared with pure Si clusters, and the strong metal-silicon interaction leads to size selectivity for the optimal size of the silicon cage for a given metal atom.[8] Structural and electronic properties of several low-lying energy isomers of isoelectronic Si_nM clusters ($M =$ Sc^-, Ti, V^+) for $n = 14$–18 have been studied by Torres *et al.*[14] using first-principles quantum mechanical calculations. The geometries, stabilities, electronic, and magnetic properties of the transition metal-doped Si_nM ($M =$ Sc, Ti, V, Cr, Mn, Fe, Co, Ni, Cu, Zn; $n =$ 8–16) clusters have also been investigated.[15] Kawamura *et al.*[12] calculated the ionization potentials and electron affinity (EA) of the Ti-, Zr-, and Hf-doped silicon clusters, as well as Raman intensity and infrared (IR) activity of Ti-doped silicon clusters. Kumar *et al.*[16] have studied in detail the bonding characteristics as well as IR and Raman spectra for $M@Si_{16}$ clusters with $M =$ Ti and Zr. Reis and Pacheco[17] have investigated the vibrational

modes and IR spectra of the exceptionally stable isovalent $X@Si_{16}$, X = Ti, Zr, and Hf clusters by using first-principles density-functional theory. Therefore, many studies have been performed on transition metal-doped silicon clusters, but there are very few studies on silicon clusters doped with Y and lanthanides even though experimental results[9,18] on these systems have become available in recent years.

Here, we have performed a detailed study of Y-doped silicon anion clusters by varying the number of silicon atoms, as PES data[9] are available on anion clusters. We find new growth behavior of these clusters by comparing our calculated results of the density of states (DOS) with the PES data. In Y-doped silicon anion clusters, the metal atom could be a *linker* between two smaller clusters, and in some other cases, cage formation is favored as in earlier studies on transition metal-doped silicon clusters so that it becomes an *endohedral* dopant such as in $Y@Si_{16}^-$ (to be discussed later). As mentioned earlier, in the size range of $25 > n > 13$ clusters of elemental silicon, Si_n, have been known[3,4] to form prolate-shaped structures in which smaller clusters are linked. Also, for a silicon cluster, generally, it is energetically more favorable to fragment into subclusters rather than remove one atom at a time. For the case of Y-doped silicon clusters, our results point to the possibility in which in some cases the Si_nY cluster is made of two smaller silicon clusters Si_m and Si_{n-m} that roughly keep their identity as in pure Si clusters but are linked with the metal atom, while in other cases the Y-Si interaction is so strong and the number of Si atom is appropriate that the atomic structure is completely transformed into an endohedral cage structure. The bonding characteristics in these growth modes are discussed. Also, we report results of Raman and IR spectra that could provide additional ways to experimentally identify the growth behavior of these clusters. Our results also suggest that higher energy isomers may be present in experiments in some cases. Neutral clusters have also been studied and are found to be important in understanding the experimental results.

The rest of the paper is organized as follows. In Sec. II, we present the computational details of our calculations. The results and discussion are given in Sec. III, and the conclusions are given in Sec. IV.

II. COMPUTATIONAL METHODS

All the calculations have been performed using the *ab initio* projector-augmented wave (PAW) pseudopotential method[19] within the density functional theory and the generalized gradient approximation[20] (GGA) for the exchange-correlation energy. For neutral clusters, we performed spin-polarized calculations, and in all cases the optimized structures are doublets due to an odd number of electrons. The pseudopotentials have been taken as implemented in the Vienna *Ab initio* Simulation Package (VASP).[21] A simple cubic unit cell with a side of 20 Å has been used for all clusters. For such large unit cells, the Γ point is used for the Brillouin zone integrations. For some cluster sizes, particularly in the range of n = 10–20, we adopted a simulated annealing approach and heated the clusters to a temperature of 1800 K for 5 ps. In this approach, the velocities of the ions were set randomly according to the Maxwell-Boltzmann distribution at a temperature of 1800 K. The temperature is defined from $T = \Sigma_i M_i |v_i|^2/[3k_B(N-1)]$ with $i = 1$ to N, M_i, the mass of the i^{th} ion, and $\boldsymbol{v}_i$, the velocity of the i^{th} ion. Here, N is the total number of atoms in the system, and we have taken here $(N-1)$ as the center of mass is conserved. Note that the cluster could rotate, keeping the center of mass fixed. The contribution from this rotation to the temperature is likely to be much smaller than the vibrational contribution and has been neglected. This is unlikely to play an important role in our case, as our purpose is to explore different configurations and not the accurate value of the temperature. From the trajectories of this run, some low-lying structures were selected and optimized using the conjugate gradient method without any symmetry constraint. In general, for all sizes a few structures were prepared either from intuition or from the available results in literature and optimized to find structures whose electronic spectra agreed with the available PES data. The lowest energy isomer of the anion is not necessarily the one that always matched the PES data.

We further reoptimized the geometries using the Gaussian 03 code,[22] particularly for cases in which (1) a slightly higher energy isomer gave better agreement with the PES results than the lowest energy isomer, and (2) some isomers were nearly degenerate in energy and whose calculated DOS, determined by PAW method, are in agreement with the experimental PES. We used the SDD[23] (Stuttgart) basis set and B3PW91 hybrid exchange-correlation functional (Becke's three-parameter hybrid functional for exchange[24] and generalized gradient functional of Perdew and Wang for correlation[20]) in the Gaussian 03 program. Calculations of the vibrational spectra with IR intensity and Raman activity have been done using the Gaussian code for the isomers whose experimental PES is in agreement with the calculated DOS, with the same level of accuracy as that for the geometry optimization to check their dynamic stability. The mode description has been made by visual inspection of the individual modes using the GaussView program. The dipole moments, polarizability, hyperpolarizability, and EA for these clusters have also been calculated.

III. RESULTS AND DISCUSSION

A. Atomic and electronic structure

We optimized a few isomers for each size of the yttrium-doped silicon anion clusters to search for the lowest energy configuration. The structural arrangements of Si_nY anion clusters for which the calculated DOS spectra are in agreement with the available experimental PES are presented in Fig. 1, and their corresponding calculated DOS spectra are shown in Fig. 2 along with the experimental results from Ref. 9. Most of these structures are of the lowest energy, except for Si_7Y^-, $Si_{10}Y^-$, $Si_{11}Y^-$, and $Si_{12}Y^-$ for which a higher energy isomer gives better agreement with PES data. We also found some isomers of Si_nY^- whose energies are very close to the lowest energy isomers. The geometrical configurations of these clusters with the lowest energy and other low-lying isomers, as obtained from VASP calculations, are shown in Fig. 3, and their corresponding DOS spectra are presented in Fig. 4. In Gaussian calculations, often the lowest energy isomer obtained from VASP calculations was also of the lowest energy. In some

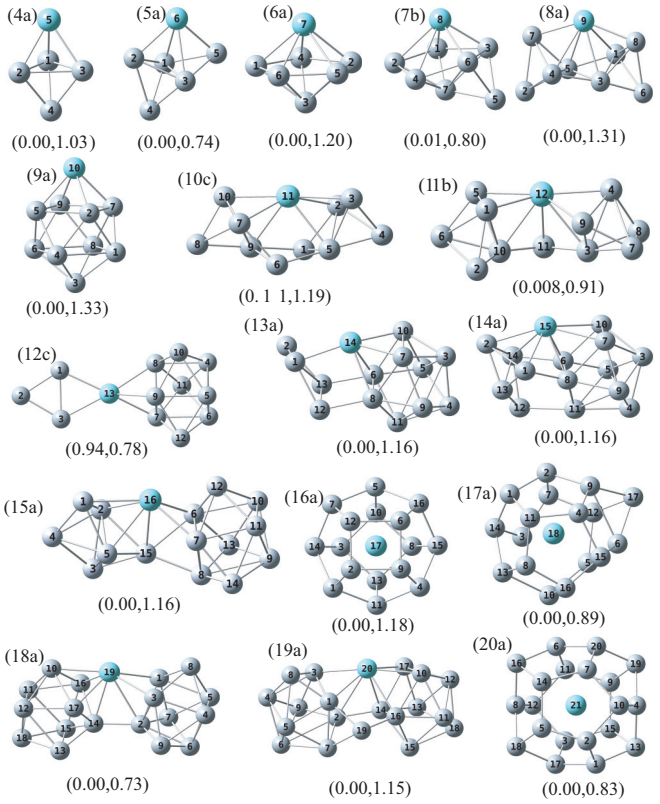

FIG. 1. (Color online) Atomic structures of Si_nY^- (n = 4–20) clusters for which the calculated DOS are in agreement with the experimental PES data. The sky blue (gray) balls represent Y (Si) atoms. Numbers on each structure show the number of silicon atoms, n, and the isomer. "a" corresponds to the lowest energy isomer and then b, c, . . . are in increasing order of energy. The metal atom has the number $n + 1$. As the size of the clusters increases, two types of growth behaviors can be noted (1) where the metal atom links two smaller clusters and (2) where the metal atom is endohedrally encapsulated by silicon atoms. In all cases, the magnetic moment is zero.

cases, the energy ordering was slightly affected, and the energy changes in such cases were up to about 0.2 eV.

For n = 4, the lowest energy isomer (4a) is a trigonal bipyramid. Its base is an equilateral triangle with the bond length of 2.774 Å. The distance between the apex metal atom and the base Si atoms is 2.713 Å, while the distance between the apex Si atom and the base Si atoms is 2.516 Å. The lowest energy isomer (5a) for n = 5 is derived by capping the lowest energy isomer of Si_4Y^-. Capping of silicon atom distorts the geometry of the trigonal bipyramid and decreases slightly the side of the base triangle facing it to 2.687 Å and results into an isosceles triangle with a side of 2.611 Å. These structures of small clusters are similar to those reported in Ref. 10. The addition of one Si atom to the lowest energy isomer of Si_5Y^- leads to the rearrangement of atoms and results into a pentagonal bipyramid structure with the metal atom capping one side of the pentagon, and it results into the lowest energy isomer (6a) for n = 6. The length of the Si-Si bonds forming the pentagon base is 2.570 Å, while the other Si-Si bond distances are 2.701 Å. These Si-Si bond distances are significantly longer compared with the bond length in tetrahedrally bonded bulk Si due to the relatively close-packed structures of these clusters. The bond length between the capping metal atom and the linked Si atoms is 2.898 Å. The calculated DOS of this isomer is in excellent agreement with the experimental PES as shown in Fig. 2. The isomer in which the metal atom is on the pentagonal base lies about 0.4 eV higher in energy. Another isomer (6b) derived by capping the lowest energy isomer of Si_4Y^- cluster (4a) by two Si atoms [Fig. 3(a)] is 0.42 eV higher in energy than (6a).

For n = 7, the lowest energy isomer (7a) forms a basketlike structure of Si atoms obtained by fusing two rhombi, and it is capped by the metal atom as shown in Fig. 3(a). Another nearly degenerate stable isomer (7b) for Si_7Y^- is derived by capping the lowest energy isomer of Si_6Y^- by a silicon atom away from the metal atom (Fig. 1), and it is 0.01 eV higher in energy than (7a). Capping of Si atom distorts the geometry of the pentagonal bipyramid structure. An isomer (7c) is obtained by fusing two silicon triangles that are linked by the metal atom and adding a silicon atom Si5 (here, the number after the Si atom is the number of the atom in the figure), as shown in Fig. 3(a). The two silicon triangles interact strongly with Si5 and the metal atom. This structure can also be viewed as two tetrahedra of Si fused together at one atom. Its energy is only slightly (0.04 eV) higher than the value for (7a); therefore, this isomer is nearly degenerate with the lowest energy structure we have obtained. Another isomer (7d) [Fig. 3(a)] originates from the lowest energy isomer of Si_6Y^- by capping a Si atom near the metal atom, and it is 0.25 eV higher in energy than (7a). For a pure Si_7 cluster, the lowest energy structure is a pentagonal bipyramid. The calculated DOS (Fig. 2) of isomers (7a) and (7b) reproduce the PES well, suggesting that these two isomers coexist in the experiment. For n = 8, the lowest energy isomer (8a) is derived by linking two silicon tetrahedra via the metal atom (Fig. 1). The two tetrahedra also interact with each other. The geometrical structures of the two tetrahedra are the same. The calculated DOS of the lowest energy isomer is in good agreement with the experimental PES (Fig. 2). The addition of one Si atom to the isomer (7d) leads to the rearrangement of atoms, and it forms the distorted structure of a pentagonal bipyramid containing a metal atom with the capping of two silicon atoms (Si2 and Si7). This gives rise to isomer (8b) shown in Fig. 3(a), and it is 0.23 eV higher in energy than (8a).

The lowest energy isomer (9a) for n = 9 is a bicapped tetragonal antiprism, and it is shown in Fig. 1. In this structure one side is capped by the metal atom and the other side by Si. The Si-Si bond lengths are in the range of 2.536–2.966 Å, while the Si-Y bond distances are 2.753 Å. Two higher energy isomers have also been obtained for Si_9Y^-. The first one (9b) is a pentagonal pyramid capped by three Si atoms (Si4, Si5, and Si9), which are further capped by the metal atom [Fig. 3(a)], and it is 0.28 eV higher in energy than (9a). The calculated DOS of the lowest energy isomer (9a) is in reasonable agreement with the experimental PES as shown in Fig. 2. Another isomer (9c), shown in Fig. 3(a), is 0.34 eV higher in energy than (9a), and it is derived by capping the isomer (7d) by two silicon atoms (Si9 and Si2). Capping of Si atoms distorts the geometry of the pentagonal bipyramid structure.

For n = 10, the lowest energy isomer (10a) is originated by linking a trigonal bipyramid and a square pyramid of Si through a metal atom, as shown in Fig. 3(a). The two silicon clusters interact with each other. Another stable isomer (10b)

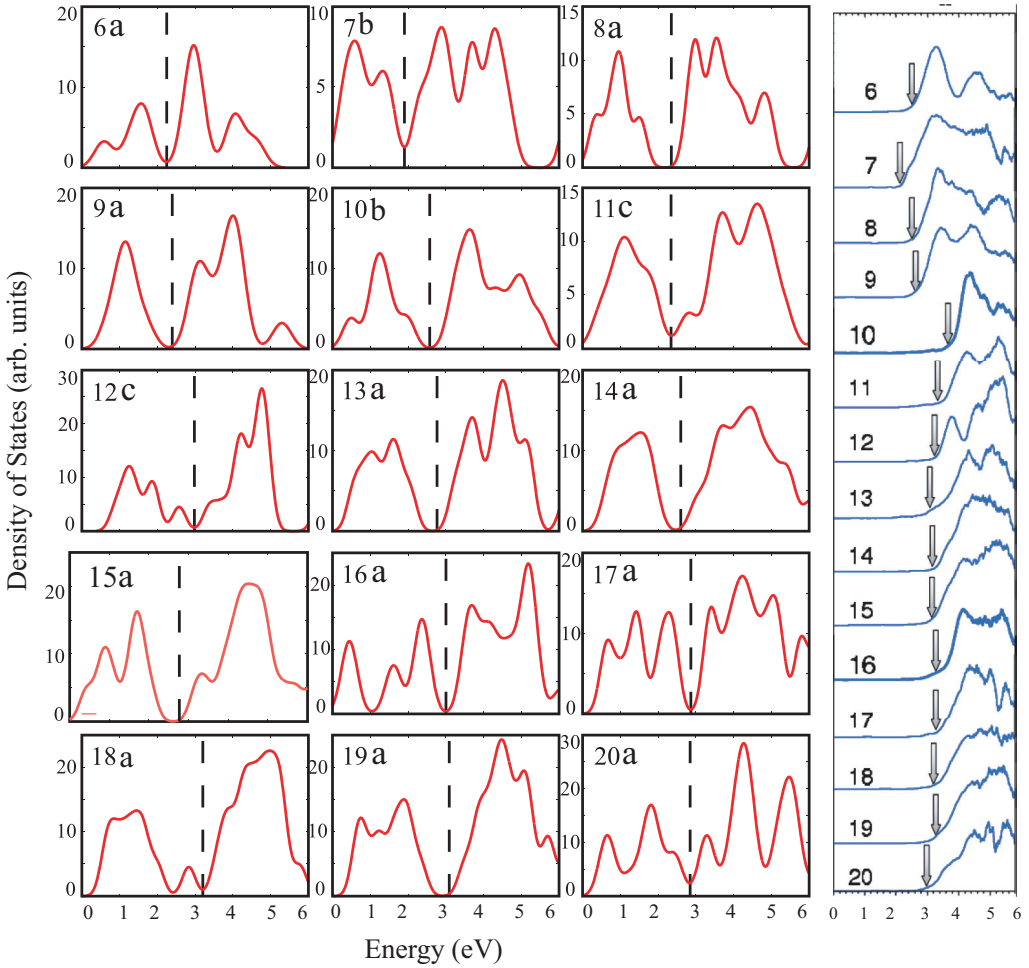

FIG. 2. (Color online) The calculated DOS of Si_nY^- clusters with $n = 6$–20 for isomers shown in Fig. 1 for which the calculated electronic spectra are close to the experimental PES data, which are shown in the extreme right column taken from Ref. 9 with permission from AIP. The calculated electronic spectra are obtained by Gaussian broadening of the electronic levels with the width of 0.25 eV. The vertical broken line shows the HOMO. In the calculated curves, a HOMO-LUMO energy gap is generally not seen at the HOMO, or it is very small compared with the actual value because of the large Gaussian broadening for the sake of comparison with the experimental PES data. Also the calculated energies are given without -ve sign.

is originated from linking of two silicon trigonal bipyramids through the metal atom, and it is shown in Fig. 3(a). It lies 0.06 eV higher in energy than (10a); therefore, it is nearly degenerate. The two Si clusters are not interacting directly with each other. The geometrical structures of the two trigonal bipyramids are identical. These results show the importance of linked clusters that compete with some close-packed basketlike structures that have been studied by Kawamura *et al.*[12] for the Zr doping case. Note that the neutral Zr-doped clusters are isoelectronic with anion Y-doped clusters. Another nearly degenerate isomer (10c) for which the calculated DOS is in agreement with the PES is derived from the lowest energy isomer (8a) of Si_8Y^-. In this isomer, two Si tetrahedra are linked by a metal atom along with two more Si atoms (Si1 and Si6) as shown in Fig. 1. The two silicon tetrahedra interact strongly with Si1 and Si6 atoms. The geometrical structures of the two tetrahedra are the same. The distance between the two added Si atoms is 3.472 Å, and they do not interact with each other directly. This structure can also be viewed in the form of two interacting Si_4 rhombi, each of which is capped by a Si atom. Note that elemental Si_4 has a rhombus structure. Another isomer (10d) is 0.19 eV higher in energy than isomer (10a), and it forms a basketlike structure with the metal atom on top of it [Fig. 3(a)].

For $n = 11$, the lowest energy isomer (11a) adopts a partial cagelike structure in which the metal atom caps on the basket of the silicon cluster shown in Fig. 3(a). A nearly degenerate isomer (11b), whose calculated DOS is in agreement with the experimental PES, is found to originate from the linking of two silicon trigonal bipyramids through the metal atom with the addition of one more Si atom (Si11), and this is shown in Fig. 1. The two silicon trigonal bipyramids interact strongly with Si11, and the linking Si atom is also interacting with the metal atom. Another stable nearly degenerate isomer (11c) also exists for $Si_{11}Y^-$, and it is a linked cluster derived from a silicon octahedron and a silicon trigonal bipyramid that are linked through the metal atom, but the two silicon clusters are not interacting directly with each other, as can be seen in Fig. 3(a).

For $n = 12$, the lowest energy isomer (12a) is derived from the linking of a Si_3 triangle and a Si_9 tricapped trigonal

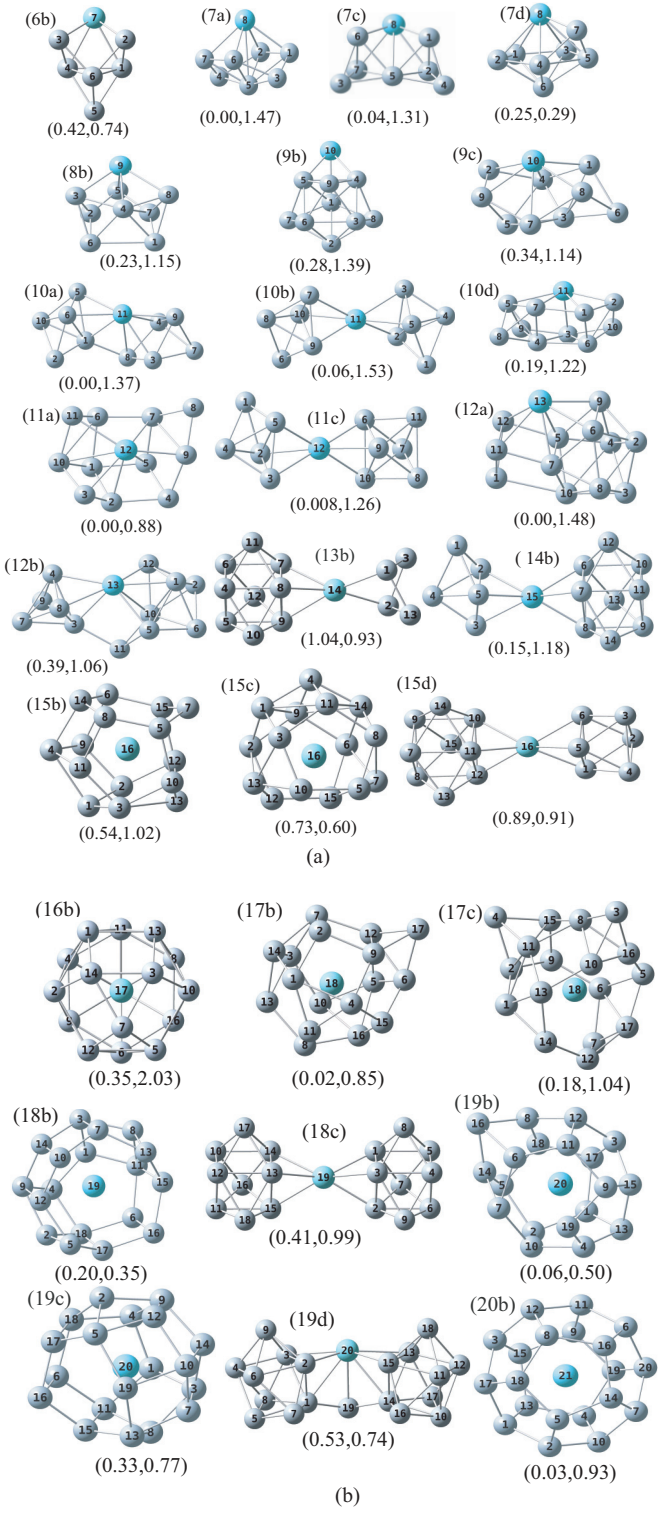

FIG. 3. (Color online) (a) Structural arrangements of some low-lying isomers of Si_nY^- clusters with $n = 6$–15. Other details are as in Fig. 1. (b) Atomic structures of some low-lying isomers of Si_nY^- clusters, $n = 16$–20. Other details are the same as in Fig. 1.

prism (TTP) via the metal atom as shown in Fig. 3(a). The triangle and TTP interact very strongly with each other. A few low-lying isomers and their DOS are given in Fig. S1 in the Supplemental Material.[25] Among these, a linked isomer [(12b) in Fig. S1 in the Supplemental Material[25]] with a rhombus-shaped Si_4 and a Si_7 subcluster interacting with the metal atom lies only 0.08 eV higher in energy than the lowest energy isomer, while a slightly different isomer [(12c) in Fig. S1 in the Supplemental Material[25]], in which the metal atom becomes part of the rhombus and interacts with a TTP, lies 0.16 eV higher in energy than (12a). Another stable isomer shown as (12b) in Fig. 3(a) lies 0.39 eV higher in energy than (12a) and is originated by the addition of two Si atoms (Si11 and Si5) to a higher energy isomer (10d) of $Si_{10}Y^-$. The two Si clusters interact with Si11 and Si5 atoms. The geometrical structures of the two trigonal bipyramids are different. The isomer (12c), shown in Fig. 1, whose DOS is in agreement with the PES is, however, 0.94 eV higher in energy than (12a), and it is found to originate from a silicon triangle and a Si_9 TTP linked through the metal atom, as shown in Fig. 1, but these two silicon clusters do not interact with each other. This higher energy isomer is possible because the TTP Si_9 cluster is a very stable structure[3] for elemental silicon clusters. The DOS of this isomer has features similar to the one observed in PES spectra, but the peak at around 5 eV in Fig. 2 is broader. This indicates that other isomers are likely to coexist. Note that the DOS of isomer (12c) in Fig. S1 (see Supplemental Material[25]) also has similar characteristics, and this isomer is quite likely to coexist. In most cases for which the calculated DOS of anion agrees with the PES data, the neutral is generally of the lowest energy, even though the corresponding anion isomer may not have the lowest energy. This shows the importance of how the clusters are produced. The neutral of isomer (12a) is also of the lowest energy, but the neutral of isomer (12c) in Fig. S1 (see Supplemental Material[25]) is only 0.08 eV higher in energy than the neutral of (12a) and is nearly degenerate, while the neutral of (12b) in Fig. S1 (see Supplemental Material[25]) is 0.24 eV higher in energy than (12a). The lowest energy isomer (13a) for $n = 13$ is originated from the linking of a silicon rhombus and a distorted capped tetragonal antiprism via the metal atom. The rhombus and antiprism interact with each other. The computed DOS for this isomer is in good agreement with the experimental PES, as seen in Fig. 2. Another isomer (13b) is 1.04 eV higher in energy, and it is obtained by linking the Si_9 TTP and the Si bent rhombus through the metal atom [Fig. 3(a)]. The two Si subclusters do not interact directly with each other. Note that these cluster sizes are small so that it is not favorable to have the metal atom endohedrally doped in a cage.

For $n = 14$, the lowest energy isomer (14a) is derived from the higher energy isomer (13b) of $Si_{13}Y^-$, and it is shown in Fig. 1. In this isomer one Si atom is added to the Si rhombus of the $Si_{13}Y^-$ cluster. The two Si subclusters interact very strongly with each other and with the metal atom. Another stable isomer (14b) is 0.15 eV higher in energy [Fig. 3(a)] and is obtained by linking a Si_9 TTP and a Si trigonal bipyramid through a metal atom. These two silicon subclusters interact strongly with the metal atom but not with each other. The computed DOS of the two isomers together (Figs. 2 and 4) reproduce the PES spectrum well, suggesting that both the isomers may contribute to the experimental PES spectrum. For $n = 15$, the lowest energy isomer (15a) is derived from the lowest energy isomer (14a) of $Si_{14}Y^-$ (Fig. 1). In this isomer, one Si atom is added to the Si_5 subcluster of $Si_{14}Y^-$. The computed DOS for this isomer is in good agreement with the

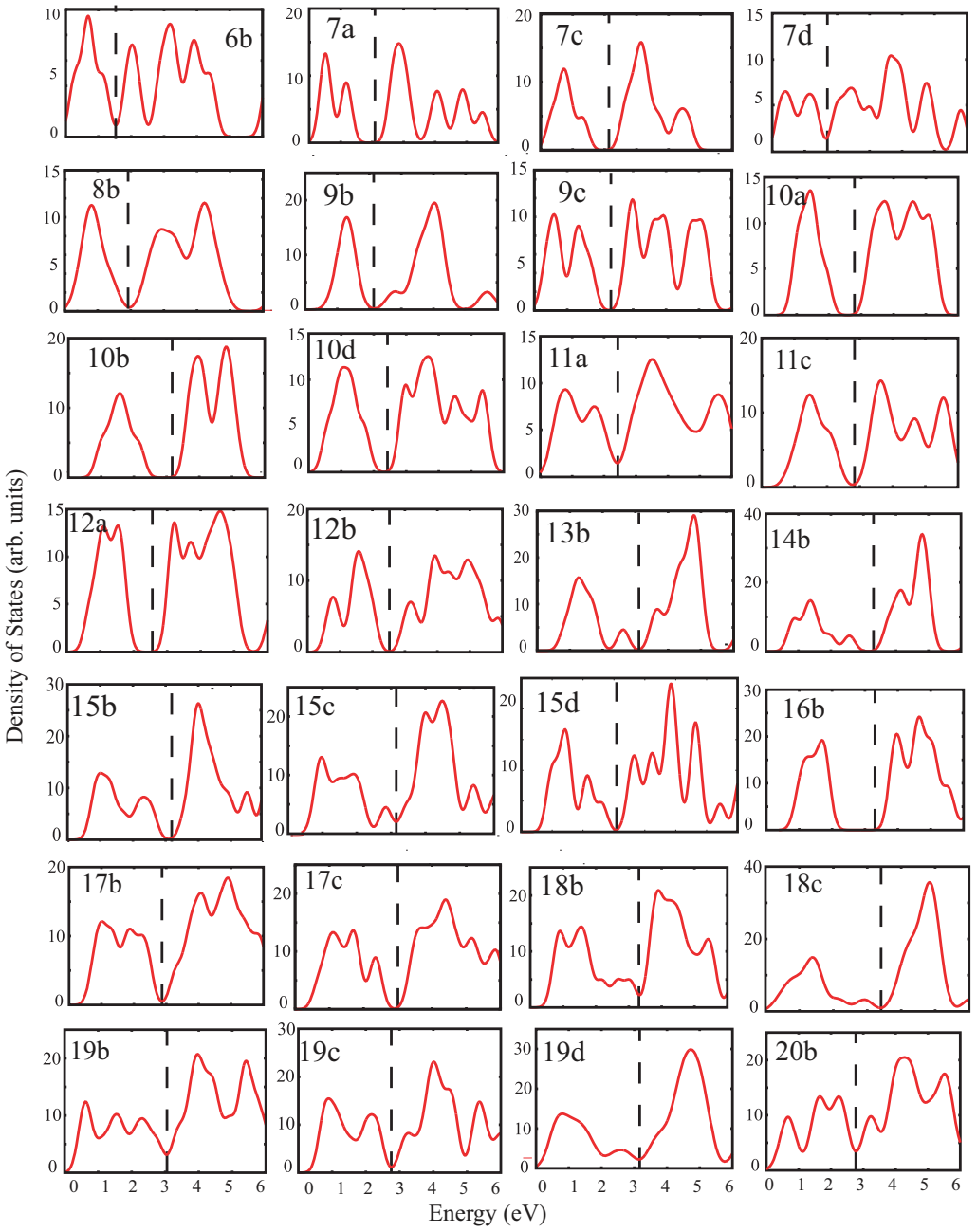

FIG. 4. (Color online) The calculated DOS of some low-lying isomers of Si_nY^- clusters, $n = 6$–20, as shown in Fig. 3. The vertical dashed line shows the HOMO. In these figures, the HOMO-LUMO energy gap is not seen, or it is much smaller than the actual value because of the large Gaussian broadening for the sake of comparison with the experimental PES data. Also the energies are given without -ve sign.

experimental PES, as seen in Fig. 2. Two other isomers (15b and 15c) are 0.54 and 0.73 eV higher in energy, respectively, than (15a). These isomers have cagelike structures, with the metal atom located inside the cage, as shown in Fig. 3(a). These results suggest that 15 Si atoms are not enough to form a lowest energy cage structure. Another isomer (15d) lies 0.89 eV higher in energy than (15a), and it is found to originate from a Si octahedron and a capped tetragonal antiprism (Fig. 1) both of which are linked through the metal atom. The two silicon subclusters do not interact with each other.

The lowest energy isomer (16a) for $n = 16$ adopts a symmetric cage structure, and the metal atom is located at the center of the cage. The cage has fullerenelike structure with eight pentagons and two squares, as was obtained by Kumar and Kawazoe[5] for $Zr@Si_{16}$, which is isoelectronic to $Si_{16}Y^-$. The Si-Si bond lengths in this structure are in the range of 2.339–2.461 Å, while the Si-Y bond lengths are 3.0 Å. The Si-Si bond lengths are much shorter than the values in smaller clusters as each Si atom has three nearest-neighbor Si atoms besides the central metal atom, and the bonding is close to the one in tetrahedrally bonded Si, which is reflected in the bond lengths. The computed DOS of this isomer is in good agreement with the measured PES (Fig. 2). Another isomer (16b), shown in Fig. 3(b), is 0.35 eV higher in energy than (16a)

and has the FK polyhedron structure with the 16 coordination and the metal atom inside. This Si polyhedron has been shown[5] to be the lowest energy structure for $Ti@Si_{16}$. However, its DOS (Fig. 4) is different from the one (Fig. 2) obtained for (16a). When compared with the PES data, it appears that both the isomers may be present in the spectrum, but the FK isomer is likely to be in a small quantity. Guo *et al.*[26] have studied doping of a lanthanide atom in Si_{16} cage and also obtained the fullerene structure to be lower in energy. We also studied a linked cluster isomer in which a capped tetragonal antiprism of Si_9 and a pentagonal bicapped Si_7 with some variations are linked with the metal atom. However, this isomer lies about 0.5 eV higher in energy than the fullerene isomer (16a). For $n =$ 17, the lowest energy isomer (17a) whose DOS is in agreement with the PES is derived from the lowest energy isomer (16a) for $n = 16$ by capping one Si atom as shown in Fig. 1. It has a distorted cagelike structure. Two other isomers (17b and 17c) are nearly degenerate in energy. Both of them have a distorted cagelike structure with the metal atom inside [Fig. 3(b)]. For $n = 18$, the lowest energy isomer (18a), whose calculated DOS is in agreement with the PES data, is obtained from two Si capped tetragonal antiprisms that are linked through the metal atom (Fig. 1). The two silicon antiprism clusters also interact with each other. The geometrical structures of the two antiprisms are slightly different. Another stable isomer (18b) is 0.20 eV higher in energy than (18a). It adopts a cagelike structure with the metal atom located inside the cage, as shown in Fig. 3(b). Another isomer (18c) is 0.41 eV higher in energy than (18a). Its structure is similar to the structure of (18a), but in this case the two Si antiprisms are not interacting with each other, and the geometrical structures of the two antiprisms are the same [Fig. 3(b)].

For $n = 19$, the lowest energy isomer (19a) is derived from the lowest energy isomer of $Si_{18}Y^-$. In this configuration the two Si antiprisms are linked by the metal atom with the addition of one Si atom Si19, as shown in Fig. 1. The two Si antiprisms are interacting with Si19 atom and with each other. The geometrical structures of the two antiprisms are different. The computed DOS of the lowest energy isomer is in excellent agreement with the PES result (Fig. 2). Three isomers of higher energy for the $Si_{19}Y^-$ cluster are shown in Fig. 3(b). The two isomers (19b) and (19c) have cagelike structures with the metal atom inside the cage, and these are 0.06 and 0.33 eV higher in energy than (19a), respectively. *These results show that the cage and linked clusters compete in this size range. This finding is very interesting as the subclusters are very stable for elemental Si clusters; therefore, our results demonstrate a new growth behavior for metal-doped silicon clusters by linking of smaller clusters, and this result could have important implication for other systems as well.* The structure of the isomer (19d) is similar to that of (19a) with a slightly different orientation, and it is 0.53 eV higher in energy than (19a).

For $n = 20$, the lowest energy isomer (20a) adopts a cagelike structure with the metal atom inside (Fig. 1). The slightly distorted icosahedral cage has 12 pentagons. The Si-Si bond lengths in the slightly distorted structure have the values in the range of 2.323–2.434 Å. This icosahedral cage structure is similar to C_{60}, but it is made of all pentagonal faces. Silicon likes pentagonal faces unlike carbon because the bonding in Si is sp^3 type, whereas in carbon fullerenes sp^2 bonding is favored. Another isomer of nearly degenerate energy (20b) also exists for the $Si_{20}Y^-$ cluster. It has an icosahedral symmetric cage structure, and the metal atom is placed inside the cage. This is similar to the earlier work of Kumar *et al.*[11] However, we found that an icosahedral symmetric structure as reported by Kumar *et al.* had a negative frequency, indicating its instability and a slightly distorted cage structure (20a) has no negative frequency. The computed DOS of the lowest energy isomer (20a) reproduces well the PES spectrum, except that in the calculated spectra there is one relatively sharp peak in between −4 and −5 eV, while in experiments there are two peaks. The DOS of isomer (20b), which is nearly degenerate with (20a), has a broader peak in the energy range of −4 to −5 eV, and the two isomers could coexist giving rise to the possibility of two peaks. Also, we found that the DOS of an isomer of $Si_{20}Y^-$ in which two clusters are linked has a peak around − 5 eV. This isomer lies about 1 eV higher in energy than isomer (20a). However, since linked clusters are favorable for smaller sizes, it is quite possible that a linked cluster isomer for $Si_{20}Y^-$ is formed even though this isomer lies much higher in energy, and this can give rise to the peak just around − 5 eV.

B. Stability of linked and endohedral caged structures

In the above discussed clusters, note that the linked cluster structures have tetrahedron as well as rhombus structure, with trigonal bipyramid, octahedron, and capped tetragonal antiprisms as subclusters, some of which are the stable structures of silicon clusters. In order to understand the stability of the linked clusters, we calculated the electronic structure of the subclusters with spin polarization, and these are shown in Fig. 5. Note that the up-spin spectrum of the

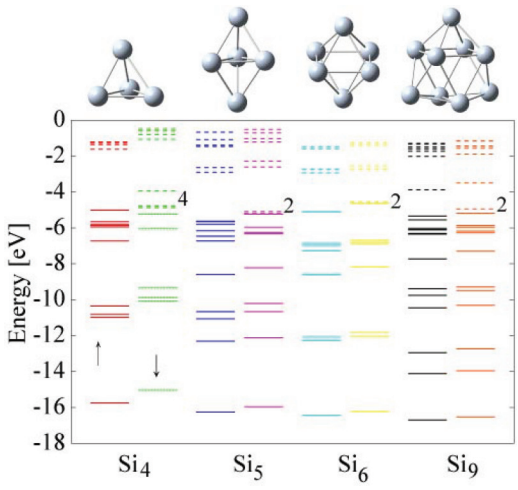

FIG. 5. (Color online) Kohn-Sham eigenstates of Si_4, Si_5, Si_6, and Si_9 clusters that are found to exist in linked clusters. Broken lines show unoccupied states. The numbers 4, 2, 2, 2 show the number of unoccupied states in the down-spin spectra below a large energy gap. These are the number of electrons that would be needed to bind in linked clusters. Atomic structures are shown above the energy spectra. The arrows show up-spin and down-spin spectra for Si_4 and similarly for other cases.

Si_4 tetrahedron has a large gap between the occupied and the unoccupied states, while in the down-spin spectrum, there are four unoccupied states, and after that there is a large energy gap. Therefore, this cluster needs four electrons to be stabilized. In the linked structure of (8a), four electrons (two electrons to each tetrahedron) are given (or shared) by Y^-, whereas the two tetrahedra are linked through two Si atoms; therefore, two electrons on each sharing Si atom contribute to the two tetrahedra, and this leads to the stability of (8a). For the trigonal bipyramid of Si_5, again the up-spin spectrum has a large gap between the occupied and the unoccupied states, while in the down-spin spectrum, there are two unoccupied states and then a large gap exists. Therefore, this isomer needs two electrons to complete a shell. As Y^- has four valence electrons, it can link two such clusters with each having two holes in the highest occupied molecular orbital (HOMO). The two trigonal bipyramids interact with Y^- so that each shares two electrons from Y^-. The electronic structure of Si_6 octahedron has features similar to those of Si_5, and accordingly in the (11b) linked isomer, two electrons of Y^- are shared with the silicon trigonal bipyramid, while the other two electrons are shared with the Si_6 octahedron. For the capped trigonal antiprism structure of Si_9, again the up-spin spectrum has a gap though smaller between the occupied and the unoccupied states, while the down-spin spectrum has two unoccupied states before a significant gap. Accordingly, this cluster needs two electrons to stabilize. This is provided by Y^- in the linked structures, as in the case of (18b). In Fig. 6, we have shown the difference in the charge density of the $Si_{15}Y^-$ cluster and the sum of the charge densities of Si_6, Si_9, and Y^- species. There is some charge transfer to Si subclusters, and there is also some covalent bonding character between the metal atom and the Si subclusters.

The stability of the cage structures has been discussed earlier by Kumar *et al.*,[8,16] and for the fullerene structure of $Y@Si_{16}$ anion in which each Si atom has three nearest-neighbor Si atoms, one can see that each Si atom has three sigma bonds with the neighboring Si atoms in the picture of sp^3 bonding, while the fourth orbital points towards outside the cage and, therefore, one can consider such 16 π-bonded electrons. Considering a spherical symmetric potential to be representative of such cages, the stability arises[16] from the filling of the 1D shell of the spherical potential. On the other hand, the stability of a close-packed FK structure [(16b) in Fig. 3(b)] can be understood[16] from the filling of the 2D shell in a spherical potential corresponding to 68 valence electrons.

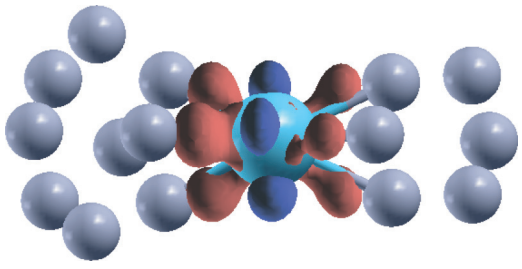

FIG. 6. (Color online) The difference of the charge densities between the $Si_{15}Y^-$ cluster and sum of the charge densities of Si_{15} and Y^- separately keeping the Si atoms and Y^- ion at the respective positions as in the $Si_{15}Y^-$ linked cluster. There is an excess charge between the Y atom and Si subclusters and depletion of the charge around the Y ion. The bonding is covalent ionic. The value of the charge density isosurface is 0.05 ($e/Å^3$).

Cluster size $Si_{15}Y^-$ is at the boundary after which cage structures start becoming favorable or the linked clusters compete with the cage isomers. We have calculated the IR and Raman spectra for the two isomers of the $n = 15$ case (Fig. 7). The calculated spectra are quite different, and this can be helpful in the identification of the isomers and the growth behavior.

C. IR and Raman Spectra

IR and Raman spectra of those isomers of Si_nY anion clusters, for which the calculated DOS is in agreement with the experimental PES, have been calculated using the B3PW91/SDD method in the Gaussian program and are shown in Fig. 8. The absence of any imaginary frequency in the spectra shows that the structures are stable. We have also calculated IR and Raman spectra for the corresponding neutral clusters, and the atomic structures for the neutral and anion clusters are nearly the same. However, a significant shift in frequency is noticed between neutral and anion clusters for some modes of vibration.

Our calculations predict that the Si_4Y^- cluster belongs to the C_{3v} point group symmetry. Two angle-bending modes of vibrations calculated at frequencies of 163 and 272 cm^{-1} and one stretching vibrational mode frequency at 288 cm^{-1} are doubly degenerate. The highly intense IR frequency at 220 cm^{-1} corresponds to an angle-bending vibration of the Si_4 cluster, whereas the highly intense Raman frequency at 312 cm^{-1} corresponds to the stretching of the three Si-Y bonds. The Si_5Y^- cluster belongs to the C_s point group symmetry. The stretching of the Si2-Y6 bond gives rise to the most intense IR peak frequency at 352 cm^{-1}, whereas the most intense peak at 237 cm^{-1} in the Raman spectrum results from the stretching of the Si5-Y6 bond. The Si_6Y^- cluster belongs to the C_{5v} point group symmetry with six doubly degenerate modes of vibration. The lowest doubly degenerate vibration mode at 123 cm^{-1} is an angle-bending mode and results in the most intense IR frequency. Three sharp peaks in the Raman spectrum calculated at frequencies 216, 262, and 348 cm^{-1} result from the angle-bending, symmetric stretching of Si-Si bonds, and breathing mode, respectively. The Si_7Y^- cluster belongs to the C_1 point group symmetry. The highest frequency at 411 cm^{-1} has the maximum intensity in the IR spectrum, and it corresponds to the stretching vibration of the Si7-Si5 bond, while the maximum Raman activity at 317 cm^{-1} results from the stretching vibration of Si6-Y8, Si4-Y8, and Si3-Y8 bonds.

The IR intensity and Raman activity for Si_nY^- clusters with $n = 8$–11 are shown in Fig. 8(b). The Si_8Y^- cluster belongs to the C_2 point group symmetry. The frequency of the butterfly mode is calculated to be 112 cm^{-1}. The strongest IR frequency at 340 cm^{-1} results from the antisymmetric stretching of Si3-Y9 and Si5-Y9 bonds, as well as antisymmetric angle bending of Si8-Y9-Si3 and Si7-Y9-Si5 together. Two sharp peaks are calculated at frequencies 354 and 457 cm^{-1} in the Raman spectrum. The first one is found to be a coupled

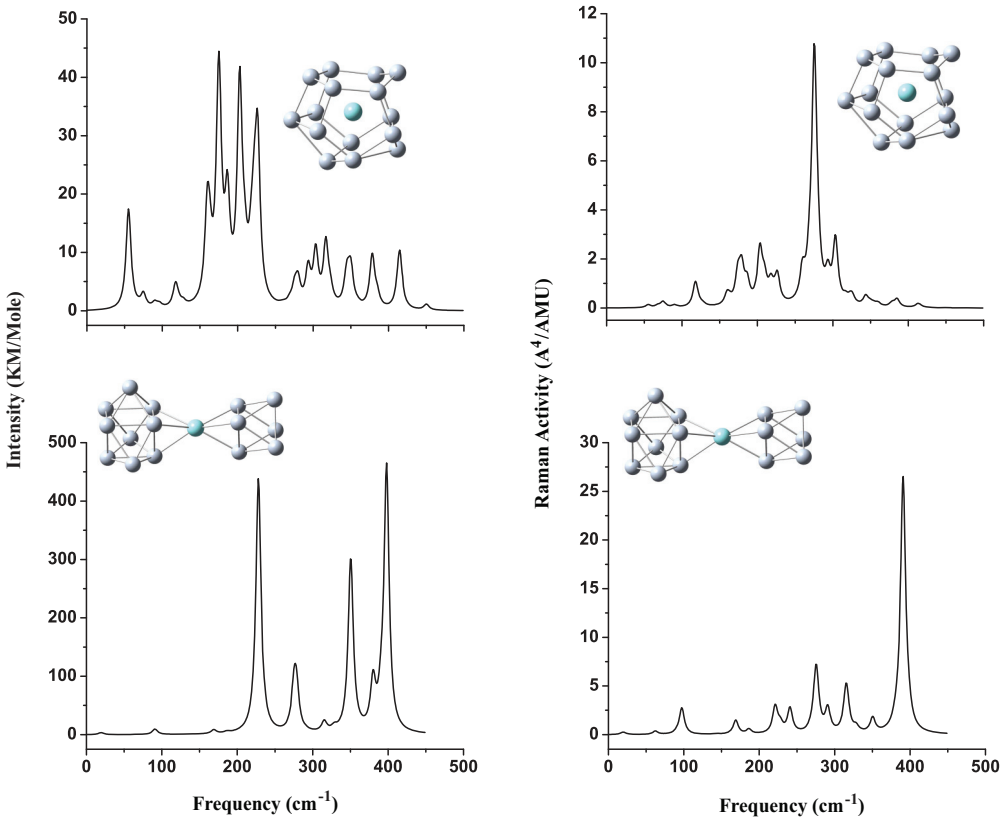

FIG. 7. (Color online) The IR intensities and Raman activities of the cage and linked isomers of the $Si_{15}Y^-$ cluster.

mode that results from the symmetric stretching of Si3-Y9 and Si5-Y9 bonds, as well as symmetric angle bending of the Si8-Y9-Si3 and Si7-Y9-Si5 together. The second mode results from the symmetric stretching of Si2-Si5 and Si3-Si6 bonds. The Si_9Y^- cluster belongs to the C_{4v} point group symmetry with six doubly degenerate modes of vibration. The highest intensity peak at 184 cm^{-1} in the IR spectrum corresponds to the symmetric angle bending of the cluster. On the other hand, in the Raman spectrum, the strongest peak at 302 cm^{-1} corresponds to the symmetric stretching of all the Si atoms linked with the metal atom. The $Si_{10}Y^-$ cluster belongs to the C_2 point group symmetry. The frequency of the butterfly mode is calculated to be 113 cm^{-1} for the $Si_{10}Y^-$ cluster and is found to be similar to the Si_8Y^- cluster. The strongest IR and Raman peaks are found at the same frequency (428 cm^{-1}) as a result of the antisymmetric and symmetric stretching of triangles Si8-Si9-Si10 and Si3-Si4-Si5, respectively. The $Si_{11}Y^-$ cluster belongs to the C_1 point group symmetry. The stretching of Si1-Si5 and Si1-Si10 bonds gives rise to the most intense IR peak at 337 cm^{-1}, whereas the stretching of Si3-Si11, Si9-Si7, and Si3-Si7 bonds gives rise to the strongest Raman peak at 439 cm^{-1}. The butterfly mode for this cluster is calculated at 35 cm^{-1}.

The IR and Raman spectra of Si_nY^- clusters with n = 12–15 are shown in Fig. 8(c). The $Si_{12}Y^-$ cluster belongs to the C_1 point group symmetry. The most intense IR peak at 245 cm^{-1} corresponds to the symmetric angle bending of the Si_3 cluster, whereas in the Raman spectrum the strongest peak at 307 cm^{-1} corresponds to the stretching of all the Si atoms that are linked with the metal atom. The butterfly mode is calculated at 18 cm^{-1}. The $Si_{13}Y^-$ cluster belongs to the C_1 point group symmetry. The stretching of Si3-Si4 and Si4-Si11 bonds give rise to the most intense peak at 325 cm^{-1} in the IR spectrum, whereas the stretching of Si6-Si13 and Si2-Si13 bonds gives rise to the strongest Raman peak at 447 cm^{-1}. The $Si_{14}Y^-$ cluster belongs to the C_1 point group symmetry. The most intense IR peak at 342 cm^{-1} corresponds to the stretching of the triangle formed by atoms Si10, Si7, and Si3, as well as the Si4-Si11 bond, whereas in the Raman spectrum the strongest peak at 291 cm^{-1} corresponds to the stretching of the triangle Si3-Si4-Si5 and triangle Si3-Si4-Si9. In this case, the twisting mode of Si_9Y^- is found to be strongly coupled with the twisting mode of the Si_5Y^- cluster. The butterfly mode frequency is calculated to be the same for $Si_{13}Y^-$ and $Si_{14}Y^-$ clusters at nearly 100 cm^{-1}. The $Si_{15}Y^-$ cluster belongs to the C_1 point group symmetry. The most intense peak at 226 cm^{-1} in the IR spectrum corresponds to the stretching of Si13-Si8 and Si14-Si8 bonds, while the strongest Raman peak at 396 cm^{-1} corresponds to the stretching of Si1, Si2, Si4, and Si5 atoms.

The IR and Raman spectra of Si_nY^- clusters with n = 16–19 are shown in Fig. 8(d). The $Si_{16}Y^-$ fullerene belongs to the D_{4d} point group symmetry with 16 doubly degenerate modes of vibration. Two peaks at 285 and 337 cm^{-1} in the Raman spectrum correspond to outer ring (made of eight atoms) breathing and the inner rings (formed by the two squares) breathing modes, respectively. The most intense IR peak at 212 cm^{-1} is a doubly degenerate mode. It results from the stretching of the outer ring atoms and the stretching of all the Si atoms that are linked with the metal atom. The $Si_{17}Y^-$ cluster belongs to the C_1

point group symmetry. The most intense IR peak at 231 cm^{-1} corresponds to the angle bending of the cluster, whereas in the Raman spectrum the strongest peak at 277 cm^{-1} corresponds to cluster breathing. The $Si_{18}Y^-$ cluster belongs to the C_s point group symmetry. In this case, the strongest IR and Raman peaks are found at the same frequency (228 cm^{-1}) that corresponds to the coupled angle bending of both the Si_9Y^- clusters. The butterfly mode for this cluster is calculated at 62 cm^{-1}. The twisting modes of the two Si_9Y^- are coupled with each other. The $Si_{19}Y^-$ cluster belongs to the C_1 point group symmetry. Similar to $Si_{18}Y^-$, the strongest IR and Raman peaks are found at the same frequency (327 cm^{-1}), which corresponds to the stretching of one of the two Si_9Y^- clusters (Si 13, 18, 12, 10, 11, 15, and 17). The second strongest Raman peak at 313 cm^{-1} is dominantly due to stretching of the Si3-Si4 bond. The frequency at 51 cm^{-1} corresponds to the butterfly mode.

The $Si_{20}Y^-$ cluster belongs to the C_i point group symmetry with 19 doubly degenerate modes of vibration. In VASP calculations, an icosahedrally symmetric isomer was also obtained, but it had negative frequencies. Therefore, a slightly deformed structure is lower in energy. IR and Raman spectra are shown in Fig. 8(c). The strongly intense peak in the IR spectrum at 212 cm^{-1} is a doubly degenerate mode, resulting from the stretching of the outer ring and stretching of all the Si atoms that are linked with the metal atom. The strongest peak in the Raman spectrum at 256 cm^{-1} corresponds to the breathing mode of the cluster.

D. HOMO-LUMO gap and the adiabatic and vertical detachment energies

The energy gap between the HOMO and the lowest unoccupied molecular orbital (LUMO) has been calculated using B3PW91/SDD, and it is shown in Fig. 9 for each cluster size whose experimental PES is in agreement with the calculated DOS. Note that the values of the HOMO-LUMO gap with the B3PW91 hybrid functional is higher compared with those obtained with VASP. A small HOMO-LUMO gap could mean enhanced reactivity and hence reduced stability. As seen from Fig. 9, the $Si_{10}Y^-$, $Si_{13}Y^-$, $Si_{16}Y^-$, and $Si_{19}Y^-$ clusters have relatively larger gaps than their neighboring clusters. In other words, from $n = 10$ onwards the successive addition of three silicon atoms results in an increase in the energy gap. A significantly large value of the HOMO-LUMO gap of 2.21 eV has been calculated for $n = 10$ within the B3PW91 hybrid functional; hence, $Si_{10}Y^-$ is more stable and less reactive as

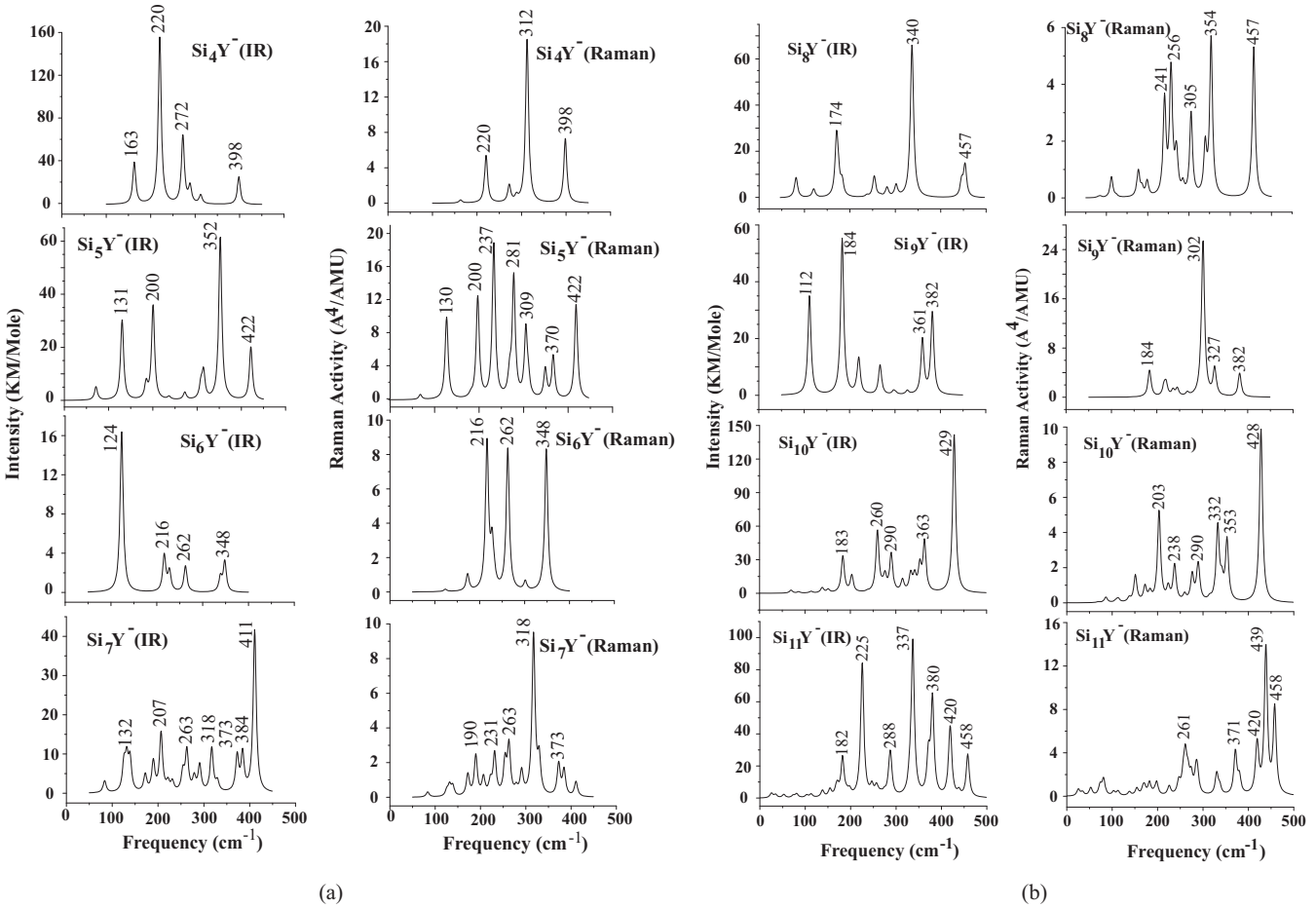

FIG. 8. (a) IR and Raman spectra of isomers of Si_nY^- ($n = 4$–7) clusters whose calculated DOS is in agreement with the experimental PES. (b) IR and Raman spectra of isomers of Si_nY^- ($n = 8$–11) clusters whose calculated DOS is in agreement with the experimental PES. (c) IR and Raman spectra of Si_nY^- ($n = 12$–15) clusters whose calculated DOS is in agreement with the experimental PES. (d) IR and Raman spectra of isomers of Si_nY^- ($n = 16$–19) clusters whose calculated DOS is in agreement with the experimental PES. (e) IR and Raman spectra of the lowest energy isomer of the $Si_{20}Y^-$ cluster whose calculated DOS is in agreement with the experimental PES.

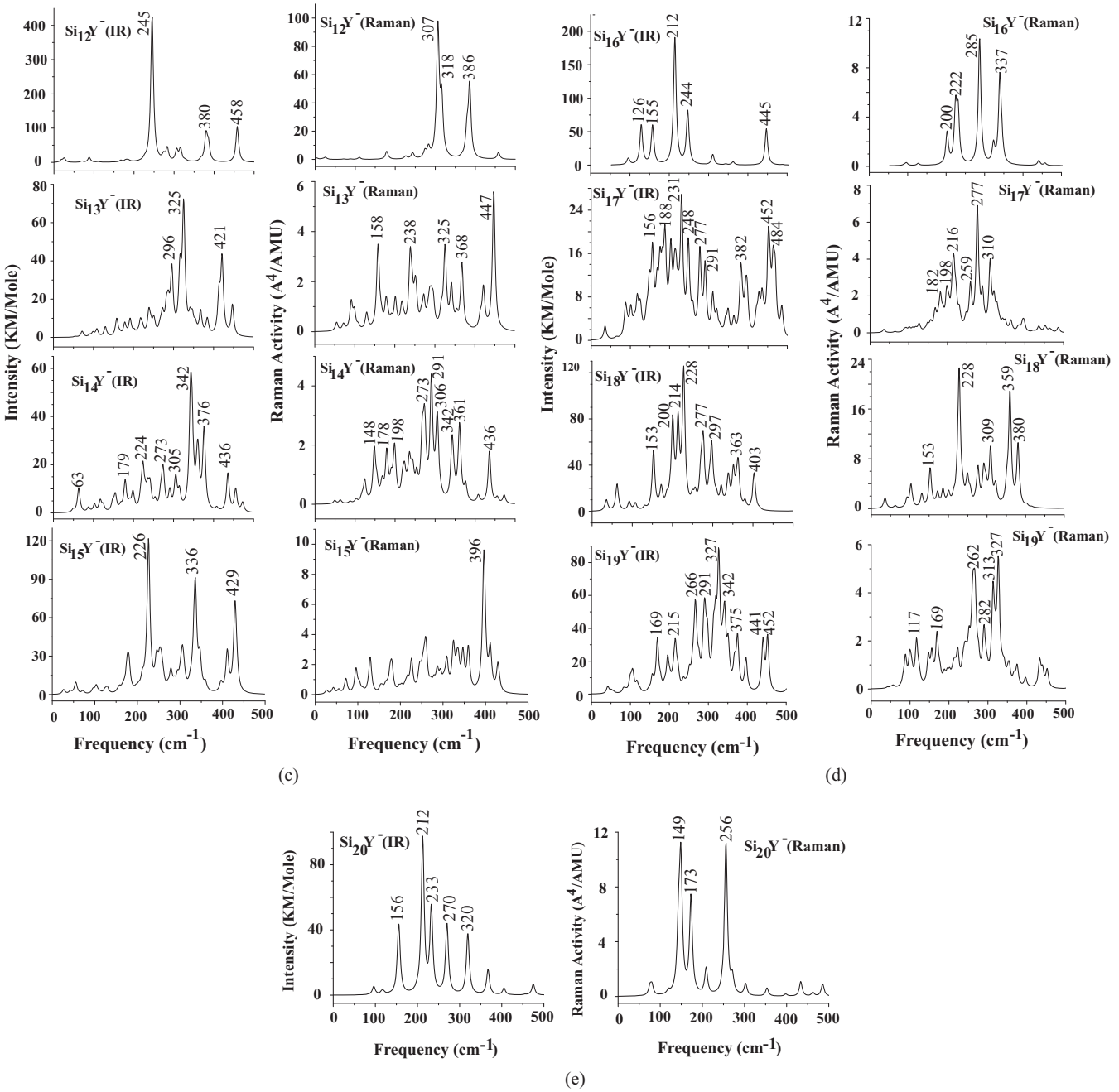

FIG. 8. (*Continued*.)

compared to other clusters. In addition to $n = 10$, a large gap is found for $n = 13$, 16, and 19 from our calculations.

The EA has been calculated using the B3PW91/SDD method for the neutral clusters, taking the difference of the energies of the optimized neutral and anion clusters. Its variation with the cluster size is shown in Fig. 9. The EA exhibits an approximate odd-even oscillation. Noticeable peaks are found at $n = 6$, 10, 12, 16, and 19, and dips are found at $n = 11$, 14, 17, and 20. The EA of the clusters with $n = 12$, 13, 16, 18, and 19 is found to be larger than the values for halogen atoms such as Cl, which has the highest EA in the periodic table, and thus, the neutral clusters behave as superhalogens.

The adiabatic detachment energy (ADE) is the difference in the total energies of the optimized geometries of the neutral and anion clusters, and therefore it is the same as the EA. The vertical detachment energy (VDE) is the difference in the total energies of the optimized geometries of the neutral cluster fixed at the anion geometry and the optimized anion. The ADE and VDE calculated using VASP are tabulated in Table I along with the available experimental results (see also Supplemental Material[25] for the values for different isomers). The calculated ADE and VDE for several clusters differ by a small amount due to the small difference in the structures of anion and neutral clusters. The calculated ADE values are in general slightly higher than the experimental values, and in a few cases, the

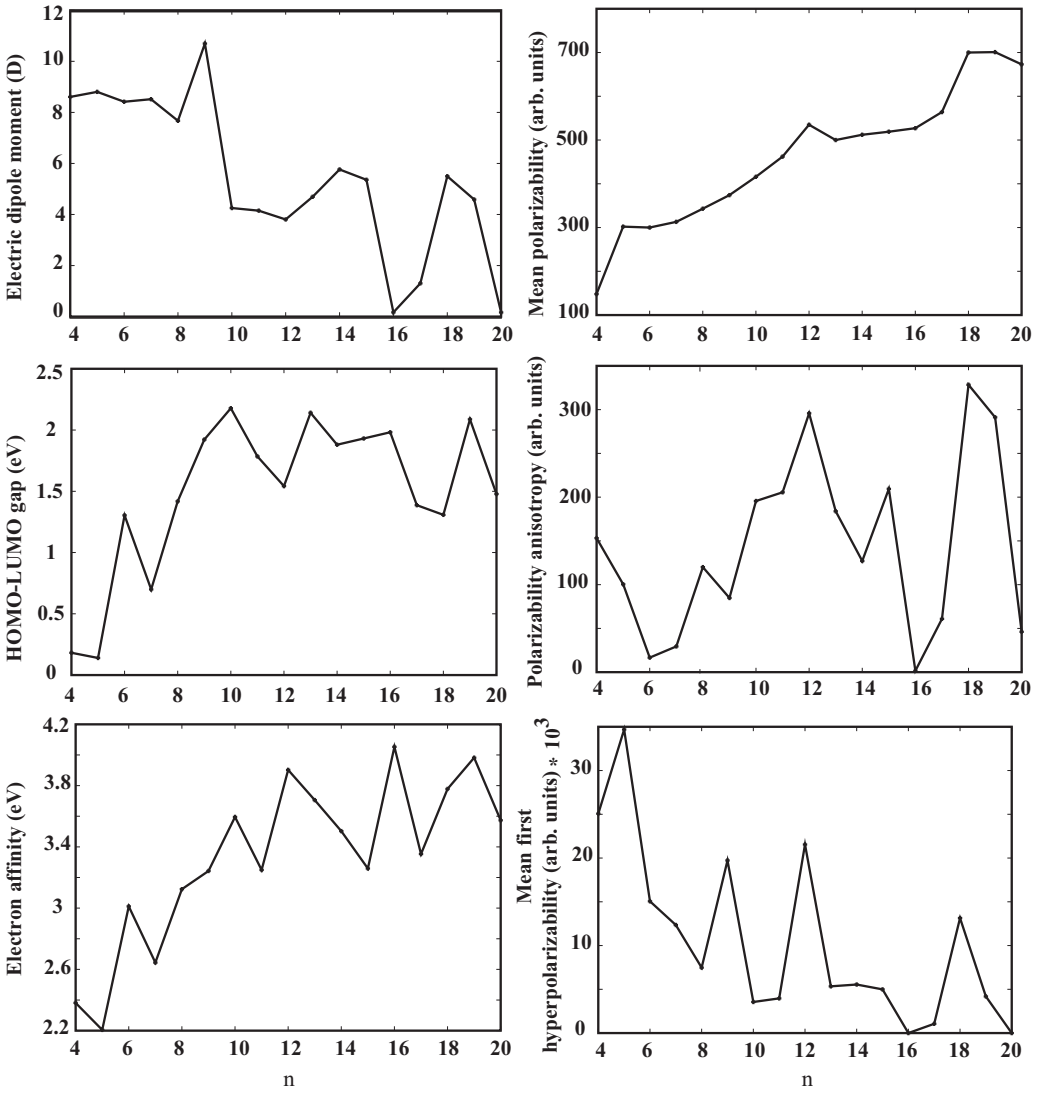

FIG. 9. Variation of the different properties of the isomers of Si_nY^- clusters as a function of the size for which the calculated DOS agrees with the experimental PES results. The EA is for the neutral clusters.

experimental value is higher than the calculated value. The overall agreement is fairly good. The values obtained from the Gaussian program are slightly higher than those obtained from the VASP program, but the trend is similar.

E. Electric dipole moments, polarizability, and hyperpolarizability

The response of a cluster in an external field can give very valuable information about the structure as well as other properties such as electric dipole moments, polarizability, and hyperpolarizability, which can be calculated. The calculated variation in the dipole moment with cluster size is shown in Fig. 9. The dipole moment depends mainly on the structural arrangement of the atoms in a cluster. It reflects the symmetry of the cluster. A small electric dipole moment represents high symmetry of the structure. As seen from the figure, the dipole moment for the clusters with $n = 16$ and 20 are nearly zero due to their symmetric cage structures. In the case of the Si_9Y^- cluster, the local dipoles on all the Si atoms, except for Si3, get cancelled out with each other, and there is a positive charge on the metal atom and negative charge on Si3 atom. This forms a large dipole moment for the Si_9Y^- cluster. It is interesting to note that the dipole moment shows even-odd oscillation for Y-doped silicon anion clusters. Clusters with an odd number of Si atoms generally have higher dipole moments than those clusters with an even number of Si atoms, with the exception at $n = 14$ and 18.

The mean polarizability α_0, the anisotropy of the polarizability $\Delta\alpha$, and the mean first hyperpolarizability β_{tot}, have been calculated using the x, y, z components from Gaussian output from the following definitions:

$$\alpha_0 = (\alpha_{xx} + \alpha_{yy} + \alpha_{zz})/3$$

$$\Delta\alpha = \tfrac{1}{2}[(\alpha_{xx} - \alpha_{yy})^2 + (\alpha_{xx} - \alpha_{zz})^2 + (\alpha_{yy} - \alpha_{zz})^2]$$

$$\beta_{\text{tot}} = [(\beta_{xxx} + \beta_{xyy} + \beta_{xzz})^2 + (\beta_{yyy} + \beta_{yzz} + \beta_{yxx})^2 + (\beta_{zzz} + \beta_{zxx} + \beta_{zyy})^2]^{1/2}.$$

The mean polarizability depends on the shape and size of the clusters. The mean polarizability of clusters generally

TABLE I. The calculated ADE and VDE of the isomers of Si_nY clusters using the PAW method for which the calculated DOS agrees with the PES data along with the available experimental results.

CLUSTER	ADE (eV) (PAW)	VDE (eV) (PAW)	ADE (eV) (GAUSSIAN)	Experiment (eV)
6a	2.798	3.008	3.012	2.5 ± 0.0043
7b	2.414	2.475	2.644	2.2 ± 0.0043
8a	2.833	2.947	3.124	2.6 ± 0.0043
9a	2.865	3.078	3.242	2.7 ± 0.0043
10c	3.186	3.279	3.595	3.6 ± 0.0043
11b	2.992	3.064	3.249	3.3 ± 0.0043
12c	3.529	3.615	3.903	3.2 ± 0.0043
13a	3.612	3.857	3.705	3.0 ± 0.0043
14a	3.097	3.198	3.503	3.1 ± 0.0043
15a	3.184	3.352	3.259	3.1 ± 0.0043
16a	3.790	3.850	4.053	2.97 ± 0.15 3.20 ± 0.10
17a	3.401	3.508	3.353	3.2 ± 0.0043
18a	3.564	3.716	3.778	3.1 ± 0.0043
19a	3.484	3.645	3.982	3.2 ± 0.0043
20a	3.333	3.485	3.573	3.0 ± 0.0043

increases with the cluster size, except at $n = 13$, and it slowly increases for 14, 15, 16, and 17, and then there is also a dip at 20. The $n = 12$ cluster has a very elongated structure, and for $n = 13$, 14, and 15, the linked clusters are relatively less spread, while for $n = 16$ there is a cage formation. Similar to 12, the $n = 18$ linked cluster is also quite elongated, while for $n = 20$, the polarizability reduces due to cage formation. Earlier studies[27] have shown that a prolate structure results in to a large polarizability. Significantly prolate configurations are preferred for $n = 12$, 18, and 19 clusters; thus, these show relatively large mean polarizabilities. The compact structures have comparatively shorter bond lengths and thus smaller volume that results in a smaller value of the polarizability for $n = 13$, 14, 15, 16, 17, and 20. Furthermore, a symmetric structure for $n = 16$ and 20 results in very low asymmetry in polarizability as well as small values of their calculated hyperpolarizability, as shown in Fig. 9. Clusters with $n = 5$, 9, 12, and 18 have very large mean hyperpolarizability, and they are likely to have interesting nonlinear properties.

IV. CONCLUSIONS

In summary we have performed *ab initio* calculations on Y-doped silicon anion clusters, and by comparing the calculated DOS with the experimental PES data, we found two growth behaviors: (1) where the metal atom acts as a linker between two subclusters and (2) where the metal atom is endohedrally encapsulated in a silicon cage. The smallest size for which an endohedral cage structure becomes favorable is 16 silicon atoms. The calculated DOS in all cases agree well with the experimental results, and this gives confidence that we have found the structures that are likely to be present in experiments. In some cases, our results suggest the presence of more than one isomer. The finding of linked clusters gives a new direction in the design of materials. Elemental silicon clusters are known to have prolate structures for the intermediate range of sizes from $n = 14$ to around 25, and their fragmentation into two subclusters is the most favorable process rather than removing atom by atom. Our finding that metal-doped silicon clusters also have prolate-shaped linked clusters suggests the possibility of new phases of materials. We may be able to develop polymeric chains in which some clusters could be linked with metal atoms. We have calculated the EA, and the values compare well with the available experimental data. Several other quantities such as the HOMO-LUMO gap, dipole moments, polarizability as well as hyperpolarizabilities, and IR as well as Raman spectra have been calculated, and these can be compared with experiments to obtain additional support for the growth behavior. Our calculations show a low-frequency mode for the linked clusters, and if observed in experiments, it could provide support for our finding of the linked clusters.

ACKNOWLEDGMENTS

V. K. gratefully acknowledges partial support from the Asian Office of Aerospace Research and Development. Part of the calculations were performed on the Param Padma Supercomputer of the Center for Development of Advanced Computing (CDAC), Bangalore, and we are grateful to the staff of CDAC for allowing the use of the supercomputer resources and their excellent support.

[1] L. Canham, Appl. Phys. Lett. **57**, 1046 (1990).

[2] See articles in V. Kumar, ed., in *Nanosilicon* (Elsevier, Oxford, 2007).

[3] K. M. Ho, A. A. Shvartsburg, B. Pan, Z. Y. Lu, C. Z. Wang, J. G. Wacker, J. L. Fye, and M. F. Jarrold, Nature (London) **392**, 582 (1998).

[4]L. Mitas, J. C. Grossman, I. Stich, and J. Tobik, Phys. Rev. Lett. **84**, 1479 (2000).
[5]V. Kumar and Y. Kawazoe, Phys. Rev. Lett. **87**, 045503 (2001).
[6]K. Koyasu, M. Akutsu, M. Masaki, and A. Nakajima, J. Am. Chem. Soc. **127**, 4995 (2005).
[7]See Chapter 3 by V. Kumar in Ref. 2, pp. 114–148.
[8]V. Kumar, Comput. Mater. Sci. **36**, 1 (2006).
[9]K. Koyasu, J. Atobe, S. Furuse, and A. Nakajima, J. Chem. Phys. **129**, 214301 (2008).
[10]A.-P. Yang, Z. Y. Ren, P. Guo, and G.-H. Wang, J. Mol. Struct. **856**, 88 (2008).
[11]V. Kumar, A. K. Singh, and Y. Kawazoe, Phys. Rev. B **74**, 125411 (2006).
[12]H. Kawamura, V. Kumar, and Y. Kawazoe, Phys. Rev. B **71**, 075423 (2005).
[13]H. Kawamura, V. Kumar, and Y. Kawazoe, Phys. Rev. B **70**, 193402 (2004).
[14]M. B. Torres, E. M. Fernández, and L. C. Balbás, Phys. Rev. B **75**, 205425 (2007).
[15]L. J. Guo, G. F. Zhao, Y. Z. Gu, X. Liu, and Z. Zeng, Phys. Rev. B **77**, 195417 (2008).
[16]V. Kumar, T. M. Briere, and Y. Kawazoe, Phys. Rev. B **68**, 155412 (2003).
[17]C. L. Reis and J. M. Pacheco, Phys. Rev. B **82**, 155440 (2010).
[18]A. Grubisic, Y. J. Ko, H. Wang, and K. H. Bowen, J. Am. Chem. Soc. **131**, 10783 (2009).
[19]P. E. Blöchl, Phys. Rev. B **50**, 17953 (1994).
[20]J. P. Perdew, in *Electronic Structure of Solids 91*, edited by P. Ziesche and H. Eschrig (Akademie Verlag, Berlin, 1991), pp. 11–20.
[21]G. Kresse and D. Joubert, Phys. Rev. B **59**, 1758 (1999).
[22]M. J. Frisch, G. W. Trucks, H. B. Schlegel, G. E. Scuseria, M. A. Robb, J. R. Cheeseman, J. A. Montgomery, Jr., T. Vreven, K. N. Kudin, J. C. Burant *et al*., Gaussian 03, Revision C.01 (Gaussian, Inc., Pittsburgh, PA, 2004).
[23]D. Andrae, U. Haussermann, M. Dolg, H. Stoll, and H. Preuss, Theor. Chim. Acta **78**, 247 (1990).
[24]A. D. Becke, J. Chem. Phys. **98**, 5648 (1993).
[25]See Supplemental Material at http://link.aps.org/supplemental/10.1103/PhysRevB.88.085412 for the atomic structures of isomers of $Si_{12}Y^-$ and the corresponding DOS. Also, the VDE and ADE values have been given for the different isomers of clusters in Table S1.
[26]L. Guo, X. Zheng, Z. Zeng, and C. Zhang, Chem. Phys. Lett. **550**, 134 (2012).
[27]J. Guan, M. E. Casida, A. M. Köster, and D. R. Salahub, Phys. Rev. B **52**, 2184 (1995).